CHEMISTRY OF MATERIALS | 25th Anniversary

Article

Molecular Engineering of Organic Sensitizing Dyes for Improved Recombination Lifetime in Solid-State Dye-Sensitized Solar Cells

William Hoang Nguyen, Colin D. Bailie, Julian Burschka, Thomas Moehl, Michael Grätzel, Michael D. McGehee, and Alan Sellinger

Chem. Mater., **Just Accepted Manuscript** • DOI: 10.1021/cm3036357 • Publication Date (Web): 15 Apr 2013

Just Accepted

Chemistry of Materials is published by the American Chemical Society. 1155 Sixteenth Street N.W., Washington, DC 20036

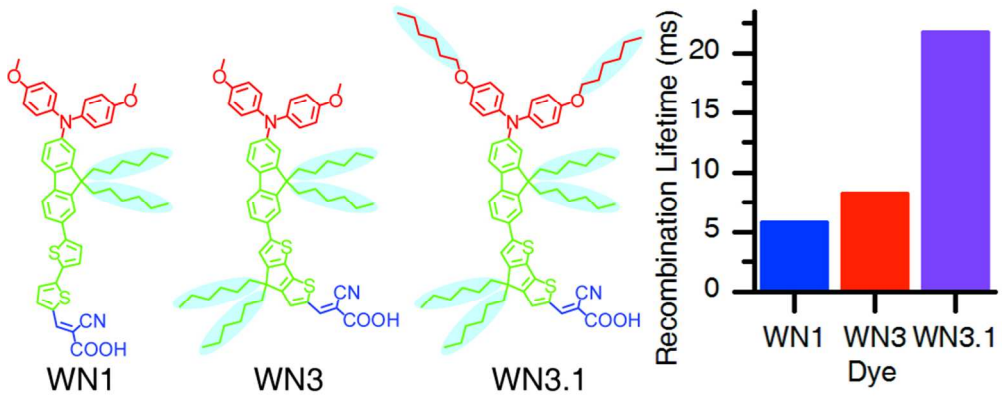

89x35mm (300 x 300 DPI)

Molecular Engineering of Organic Sensitizing Dyes for Improved Recombination Lifetime in Solid-State Dye-Sensitized Solar Cells

William H. Nguyen[‡§], Colin D. Bailie[‡†], Julian Burschka[||], Thomas Moehl[||], Michael Grätzel[||], Michael D. McGehee[†*], Alan Sellinger[°^]

[‡]These authors contributed equally to this work

[§]Department of Chemistry, Stanford University, Stanford, CA 94305, USA

[†]Department of Materials Science and Engineering, Stanford University, Stanford, CA 94305, USA

[||]Laboratoire de Photoniques et Interfaces, Institut des Sciences et Ingénierie Chimiques, École Polytechnique Fédérale de Lausanne, Station 6, 1015 Lausanne, Switzerland

[°]Department of Chemistry and Geochemistry, Colorado School of Mines, Golden, CO 80401, USA

Supporting Information Placeholder

ABSTRACT: A major limitation of solid-state dye-sensitized solar cells is a short electron diffusion length due to fast recombination between electrons in the TiO_2 electron-transporting layer and holes in the 2,2',7,7'-tetrakis(*N,N*-di-*p*-methoxyphenylamine)-9,9'-spirobifluorene (Spiro-OMeTAD) hole-transporting layer. In this report, the sensitizing dye that separates the TiO_2 from the Spiro-OMeTAD was engineered to slow recombination and increase device performance. Through the synthesis and characterization of three new organic D-π-A sensitizing dyes, WN1, WN3, and WN3.1, the quantity and placement of alkyl chains on the sensitizing dye were found to play a significant role in the suppression of recombination. In solid-state devices using Spiro-OMeTAD as the hole-transport material, these dyes achieved the following efficiencies: 4.9% for WN1, 5.9% for WN3, and 6.3% for WN3.1 compared with 6.6% achieved with Y123 as a reference dye. Of the dyes investigated in this study, WN3.1 is shown to be the most effective at suppressing recombination in solid-state dye-sensitized solar cells by using transient photovoltage and photocurrent measurements.
KEYWORDS: Dye sensitized solar cells (DSSC), recombination, organic photovoltaics (OPV)

William H. Nguyen, Colin D. Bailie, Julian Burschka, Thomas Moehl, Michael Grätzel, Michael D. McGehee[*], Alan Sellinger[^]

Molecular Engineering of Organic Sensitizing Dyes for Improved Recombination Lifetime in Solid-State Dye-Sensitized Solar Cells

Three new organic donor-π-acceptor sensitizing dyes were synthesized to understand the role of alkyl chains on recombination lifetime in solid-state dye-sensitized solar cells.

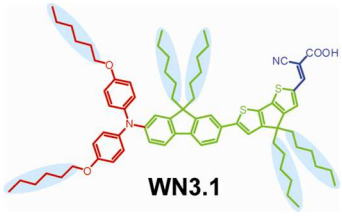

INTRODUCTION

Since the report by O'Regan and Grätzel in 1991, dye-sensitized solar cells (DSSCs) have emerged as a potential low-cost alternative energy solution compared to the typical silicon-based p-n junction solar cell.[1–4] Two general classes of dyes exist, metal-based and metal-free. Metal-free dyes are advantageous due to their high molar extinction coefficients, ease of modification and engineering, lower cost and environmental impact, and increased performance in solid-state dye-sensitized solar cells (ssDSSCs).[5,6] Typically, metal-free sensitizers belong to a class of dyes commonly referred to as D-π-A dyes, and consist of three groups: an electron donor (D); an electron-rich conjugated bridging group (π); and an electron acceptor (A) which also serves to chemically bind the dye to the surface of the TiO_2.

The operating principle of a ssDSSC is depicted in Figure 1. While process 3 is orders of magnitude faster than process 6 in ssDSSCs, process 5 is on the same time-scale as process 4, causing it to be a significant loss mechanism.[7,8] Recombination losses in ssDSSCs have led in part to an optimized device thicknesses around 2 μm[9], in a tradeoff between light absorption, charge collection efficiency, and pore-filling.[10,11] Two potential methods of addressing the losses caused by process 5 are to increase either the charge transport rate or charge carrier recombination lifetime. This paper focuses on improving recombination lifetime.

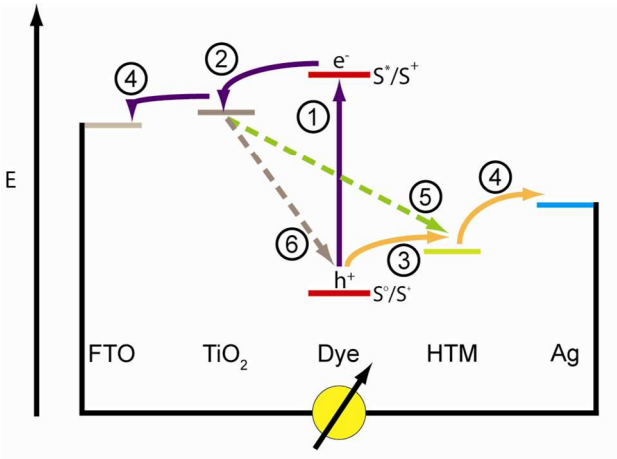

Figure 1. The operating principle of a ssDSSC. 1) Upon absorption of light, the dye generates an exciton; 2) the excited electron is injected into the conduction band of the TiO_2; 3) the dye is regenerated by the hole-transporting material (HTM); 4) the charges percolate to the electrodes. Two common back-reaction processes in ssDSSCs are: 5) recombination of the electrons in the TiO_2 with the holes in the HTM and 6) reduction of the oxidized dye.

Previous studies have shown that additional alkyl chains and increased alkyl chain length on a dye increased recombination lifetime in liquid cells. Li et al. and Paek et al. showed that two pairs of hexyl chains were more effective than one, and Kroeze et al. showed that chain lengths up to 9 carbons increased recombination lifetime.[12–14] With regard to solid-state cells, studies have shown mixed results for lengthening the alkyl chains beyond six carbons. Schmidt-Mende et al. reported on ruthenium-based dyes, with nonyl and tridecyl chains exhibiting longer recombination lifetimes than methyl, hexyl, and octadecyl chains.[15] Conversely, Moon et al. reported on organic D-π-A dyes, with hexyl chains exhibiting longer recombination lifetime than methyl or dodecyl chains.[16] In addition to the uncertainty of the ideal carbon chain length, the role of chain position and quantity in solid-state cells remains uninvestigated.

This paper aims to elucidate the effects of the quantity and position of sensitizing dye alkyl chains on the device performance of ssDSSCs with the synthesis of a series of dyes, WN1, WN3, and WN3.1 (Figure 2). The WN series of dyes were designed with D21L6[16] and C218[12] as the parent dyes due to their status as the most highly performing D-π-A dyes in solid-state and liquid DSSCs, respectively, when this study was initiated. At the time of its introduction, D21L6 broke grounds as the most efficient organic sensitizing dye used in a solid-state device.[16] Due to its well-designed D-π-A structure, D21L6 was able to achieve a relatively high molar extinction coefficient as well as efficient charge injection and electron lifetime, resulting in a power conversion efficiency (η) of 4.4% in a solid-state device. C218, a dye based on D21L6, was able to achieve a solid-state device η of 5.6% by fusing the bithiophene π-group of D21L6.[17] The fused bithiophene π-group increased the short-circuit current (J_{SC}) of the C218 device compared to that of D21L6 by red-shifting the visible light absorption maximum of the dye as well as increasing its molar extinction coefficient almost two-fold. The lower

charge recombination rate observed in liquid-state devices made with C218 compared to those with D21L6 also resulted in a higher open-circuit voltage (V_{OC}).[12]

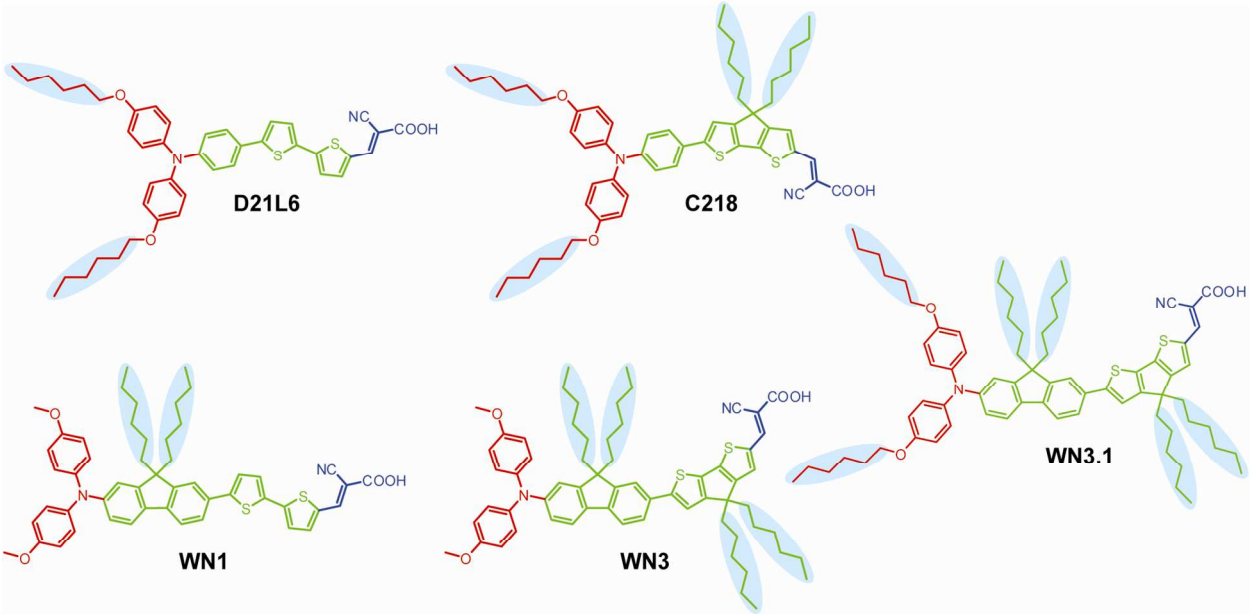

Figure 2. Chemical structures of D21L6, C218, WN1, WN3, and WN3.1 with the alkyl chains denoted with blue circles, and the donor- (red), π- (green), and acceptor-groups (blue) color coded.

The WN dyes were designed with a fluorene π-group in place of the phenyl π-group found in D21L6 and C218 to allow for the addition of an extra pair of hexyl alkyl chains along the π-backbone. Excluding the fluorene group, the π-backbone of WN1 is analogous to D21L6, while that of WN3 and WN3.1 are analogous to C218. However, WN1 and D21L6 differ in the location of their single pair of alkyl chains; WN1 has one pair of alkyl chains along the π-backbone while D21L6 has its pair of alkyl chains on the phenylamine donor-group. WN3 and C218 both have two pairs of alkyl chains; in the case of WN3, both are located on the π-backbone while C218 has one pair on the donor-group and one pair on the π-backbone. WN3.1 has three pairs of alkyl chains, one on the donor-group and two on the π-backbone. In this work, we demonstrate that recombination lifetime in ssDSSCs is linked to the quantity and position of alkyl chains and introduce a dye that is highly effective at suppressing recombination in solid-state dye-sensitized solar cells.

EXPERIMENTAL

Synthesis. Detailed synthetic preparation and characterization procedures of WN1, WN3, and WN3.1 can be found in the Supporting Information.

Scheme 1: Synthesis of WN1[a]

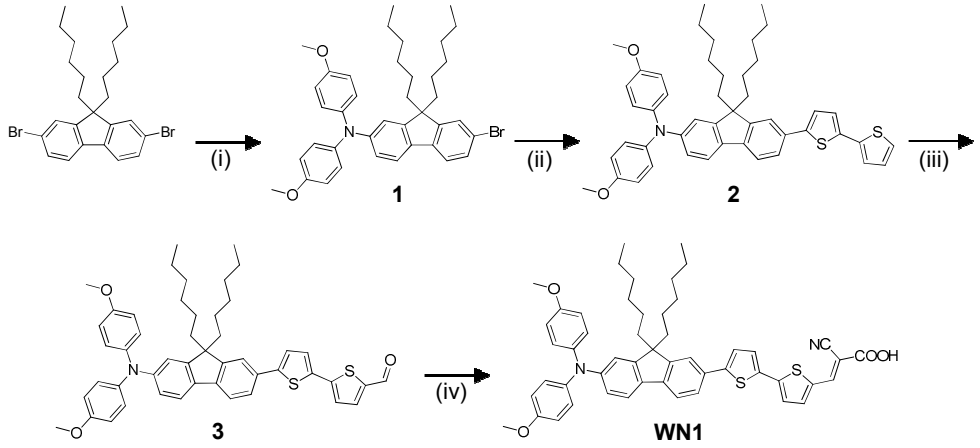

[a] (i) 4,4'-dimethoxydiphenylamine, NaO^{t}Bu, DPPF, Pd(dba)$_2$, toluene, 80 °C. (ii) 2,2-bithiophene-5-boronic acid pinacol ester, Pd(dba)$_2$, P(o-tyl)$_3$, tetraethylammonium hydroxide, toluene, 85 °C. (iii) DMF, $POCl_3$, 1,2-dichloroethane, 0-70 °C. (iv) cyanoacetic acid, piperidine, acetonitrile, 80 °C.

Scheme 2: Synthesis of WN3[a]

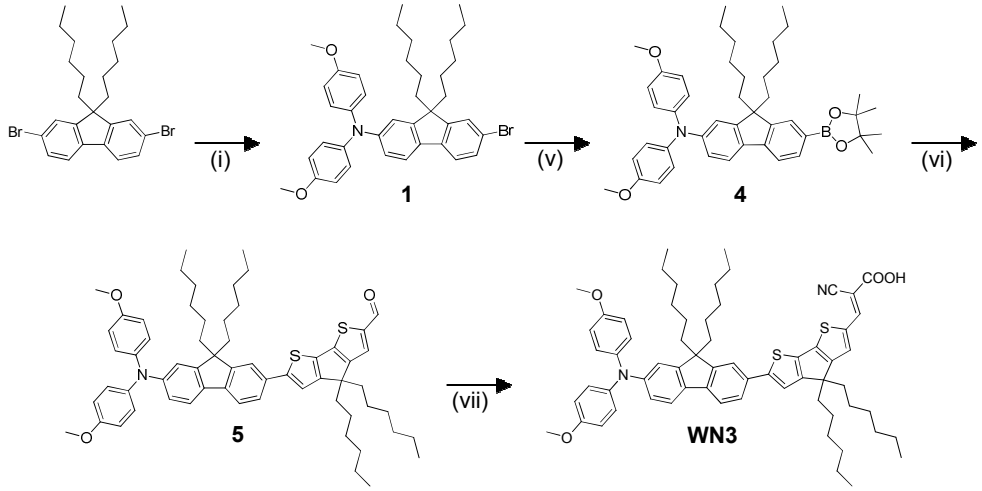

[a] (i) 4,4'-dimethoxydiphenylamine, NaO^{t}Bu, DPPF, Pd(dba)$_2$, toluene, 80 °C. (v) bis(pinacolato)diboron, $PdCl_2$(dppf), KOAc, dioxane, 95 °C. (vi) 6-bromo-4,4-dihexyl-4H-cyclopenta[2,1-b:3,4-b]-dithiophene-2-carbaldehyde, Pd(PPh$_3$)$_4$, K_2CO_3, toluene, 78 °C. (vii) cyanoacetic acid, piperidine, acetonitrile, 85 °C.

Scheme 3: Synthesis of WN3.1[a]

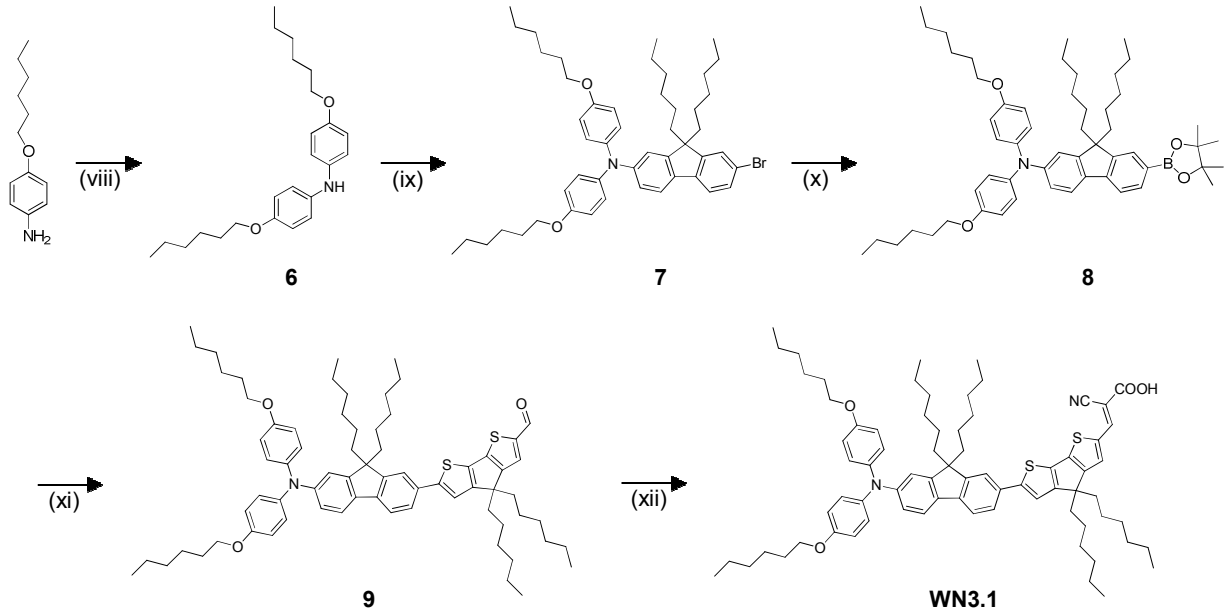

[a] (viii) 1-bromo-4-n-hexyloxybenzene, NaO^{t}Bu, DPPF, Pd(dba)$_2$, toluene, 80 °C. (ix) 9,9-dihexyl-2,7-dibromofluorene, NaO^{t}Bu, DPPF, Pd(dba)$_2$, toluene, 80 °C. (x) bis(pinacolato)diboron, $PdCl_2$(dppf), KOAc, dioxane, 95 °C. (xi) 6-bromo-4,4-dihexyl-4H-cyclopenta[2,1-b:3,4-b′]-dithiophene-2-carbaldehyde, $Pd(PPh_3)_4$, K_2CO_3, toluene, 78 °C. (xii) cyanoacetic acid, piperidine, acetonitrile, 80 °C.

Cyclic Voltammetry. Cyclic voltammetry was measured on a Bio-Logic VMP3 using a 0.1 M tetrabutylammonium hexafluorophosphate supporting electrolyte in dichloromethane with a glassy carbon working electrode, platinum counter electrode, and Ag/AgCl mesh reference electrode. A ferrocene internal reference (-5.1 V from vacuum) was used.

UV-Vis. UV-Vis spectra were measured in chloroform using a 1 cm path length cuvette (Spectrocell RF-3010-T) and a Cary 6000i UV-Vis-NIR spectrophotometer.

Emission. Emission spectra were collected in chloroform using a 1 cm path length cuvette (Spectrocell RF-3010-T) and a Horiba Jobin-Yvon Spex Fluorolog-3 fluorimeter with a 450W Xenon lamp (230-1800 nm), double grating excitation and emission monochrometers, and a 2 X thermoelectrically cooled R928P detector (240-850 nm).

Device Fabrication.[20] Fluorine-doped tin oxide glass substrates (TEC15, Pilkington) were patterned by etching with zinc powder and 2 M hydrochloric acid. After cleaning the substrates by ultrasonication in water and a UV/ozone treatment, a compact TiO_2 layer was deposited by spray pyrolysis of titanium bis(acetylacetonate)diisopropoxide solution dissolved in ethanol (1:10 volume ratio) at 450 °C using oxygen as a carrier gas. After cooling to room temperature the substrates were treated in a 0.02 M aqueous solution of $TiCl_4$ for 30 min at 70 °C, rinsed with deionized water and dried at 450 °C for 15 min. A 2.1-2.3 µm thick mesoporous TiO_2 layer was then deposited on the substrate by screen-printing, dried at 125 °C, gradually heated to 500 °C and then baked at this temperature for 15 min. The aforementioned treatment in aqueous $TiCl_4$ solution was repeated. Synthesis of TiO_2 colloid (basic route) according to J. Am. Ceram. Soc. 1997, 80(12) pp 3157-3171. Paste preparation according to Prog. Photovolt: Res. Appl. 2007; 15:603–612. Paste Characteristics from BET: Average Particle Size 23nm, Average Pore Diameter 32nm.

Prior to sensitization the TiO_2 substrates were heated to 500 °C for 30 min. After cooling to approximately 70 °C, the substrates were immersed into a 10^{-4} M solution of the sensitizer in a mixture of acetonitrile and tert-butyl alcohol (1:1 volume ratio) for 1-1.5hr. The hole-transporting material was deposited by spin-coating at 2000 rpm for 30 s with an acceleration of 330 rpm/s. The formulation of the spin-coating solution was 0.15 M (2,2',7,7'-tetrakis(N,N-di-p-methoxyphenylamine)-9,9-spirobifluorene) (spiro-OMeTAD), 0.02 M lithium bis(trifluoromethylsulfonyl)imide (LiTFSI) pre-dissolved as a 170mg/mL solution in acetonitrile, 0.12 M 4-tertbutylpyridine (TBP) in chlorobenzene, and tris(2-(1*H*-

pyrazol-1-yl)-4-tert-butylpyridine)cobalt(III) tris(bis(trifluoromethylsulfonyl)imide)) (FK209)[3], pre-dissolved in acetonitrile and added as 1.6 mol% relative to the spiro-OMeTAD concentration. Finally, 200 nm of silver was thermally evaporated on top of the device to form the back contact. The devices were sealed using a 25 μm thick polymer spacer (Surlyn, DuPont) and a microscope cover slide. The edges of the microscope cover slide were additionally sealed with two-component epoxy glue. The devices were fabricated and sealed in a dry atmosphere.

Device characterization. Current-Voltage characteristics of the cells were measured using a Keithley model 2400 digital source meter to record the generated photocurrent upon the application of an external potential bias. The irradiation source was a 450 W xenon lamp (Oriel), equipped with a Schott K113 Tempax sunlight filter to reduce the mismatch between the emission spectrum of the lamp and AM1.5G standard. The external quantum efficiency (EQE) was recorded as a function of the wavelength using a Model SR830 DSP Lock-In Amplifier (Stanford Research Systems) at a constant white light bias of approximately 10 mW/cm^2. A 300 W xenon lamp (ILC technology) was used to provide an excitation beam, which was focused through a Gemini-180 double monochromator (Jobin Yvon Ltd.) and chopped at approximately 2 Hz.

Transient Photovoltage and Photocurrent decay measurements.[17] An array of diodes (Lumiled model LXHL-NWE8 white star) was used to generate a white light bias and a perturbation excitation was produced using a red light pulsed diode (LXHLND98 redstar, 0.2 s

square pulse width, 100 ns rise and fall time) controlled by a fast solid-state switch. The voltage and current dynamics were monitored via a Keithley sourcemeter. The voltage decay measurements were conducted at zero-current conditions (V_{OC}) with varying white light bias intensities to generate different V_{OC}s. at fixed current intervals along the photocurrent-voltage curve. Similarly, the photocurrent transient decay measurements were conducted at zero-bias conditions (J_{SC}) to determine the differential charge density and extract the capacitance for each light bias condition.

RESULTS AND DISCUSSION

Replacement of the phenyl π-group with the 9,9-dihexylfluorene group blue-shifted the absorption maxima of WN1, WN3, and WN3.1 with respect to their analogous dyes, D21L6 and C218 (Figure 3a). This may be explained by a slight increase in the dihedral angle, approximately two degrees, between the fluorene and thiophene π-groups of the WN dyes versus the dihedral angle between the phenyl and thiophene π-groups of D21L6 and C218, as determined from the optimized gas-phase geometry using density functional theory, performed with Gaussian 09[18] and a B3LYP/6-31G* basis set (Figure 4 provides an example comparison of C218 and WN3.1; Figure SI4 contains the complete series of dyes; dihedral angles recorded in Table 1). Such an increase of the dihedral angle of the WN series of dyes would reduce the effective conjugation along the π-backbone, thereby increasing the HOMO-LUMO offset ($E_{(0-0)}$) and blue-shifting the absorption maximum.

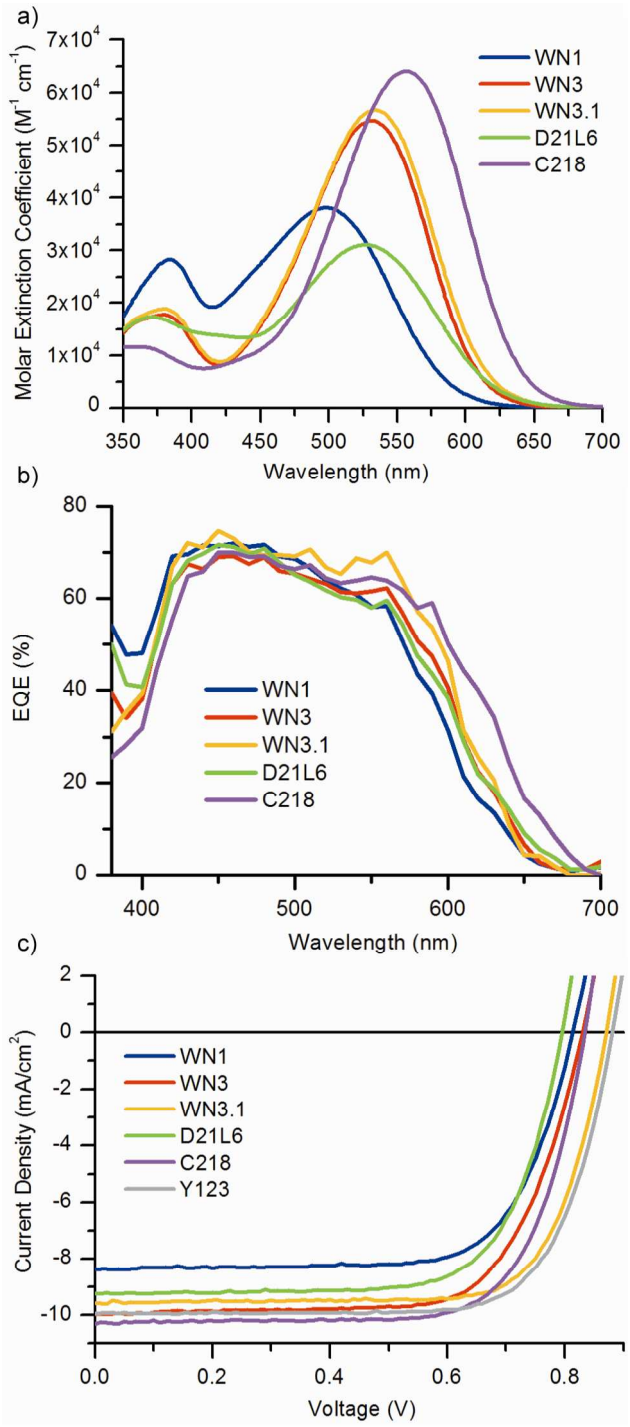

Figure 3. a) Absorption spectra of WN1, WN3, WN3.1, D21L6, and C218 in chloroform. b) EQE spectra of ssDSSCs sensitized with WN1, WN3, WN3.1, D21L6, and C218 measured under monochromatic light with a 10mWcm^{-2} white light bias. c) J-V curves of ssDSSCs sensitized with WN1, WN3, WN3.1, D21L6, C218, and Y123 measured under 100mWcm^{-2} AM1.5G illumination intensity.

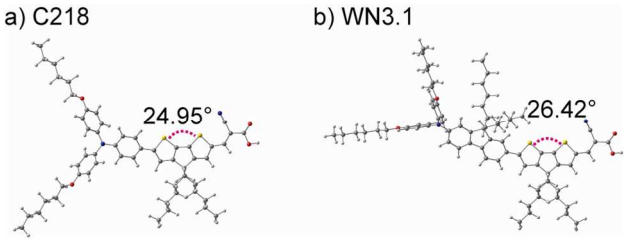

Figure 4. Dihedral angle between a) phenyl and fused bithiophene π-groups of C218 and b) fluorene and fused bithiophene π-groups of WN3.1 as determined from the optimized gas-phase geometry using density functional theory, performed with Gaussian09 and a B3LYP/6-31G* basis set.

Table 1. Absorption and Electrochemical Properties of WN1, WN3, WN3.1, D21L6, and C218

Dye	$\lambda_{max}/\varepsilon$[a] (nm)/($M^{-1}$ cm^{-1})	$E_{(S+/S)}$[b] (V)	$E_{(0-0)}$[c] (eV)	$E_{(S+/S^*)}$[d] (V)	θ[e] (°)
WN1	498/38100	-5.25	2.08	-3.17	23.89
WN3	531/54600	-5.28	1.99	-3.28	26.79
WN3.1	534/56700	-5.25	1.98	-3.27	26.42
D21L6	526/31000	-5.32	1.95	-3.36	21.96
C218	556/64000	-5.26	1.91	-3.35	24.95

[a]Absorption spectra measured in chloroform. [b]The oxidation potential, relative to vacuum, was measured using cyclic voltammetry with a ferrocene reference (-5.1 V vs. vac.). [c]The zero-zero excitation energies were estimated from the intercept of the normalized absorption and emission spectra. [d]The excited state oxidation potentials, relative to vacuum, were derived from the equation: $E_{(S+/S^*)} = E_{(S+/S)} + E_{(0-0)}$. [e]The dihedral angle between the fluorene and thiophene π-groups for WN1, WN3, and WN3.1 and between the phenyl and thiophene π-groups for D21L6 and C218 were calculated using Gaussian 09 in the gas-phase using DFT with a B3LYP/6-31G* basis set.

The J-V curves of the ssDSSCs investigated in this study are shown in Figure 3c, with the standard metrics of these curves listed in Table 2. All devices were doped with the Co(III) dopant FK209[19] at a 1.6% molar ratio with respect to Spiro-OMeTAD and light-soaked to achieve optimum efficiency. The J_{SC} can be largely explained by the position of the absorption maximum of the dyes in Table 1. A relative red-shift of a dye's absorption spectrum compared to another dye allows the dye to absorb a larger portion of the solar spectrum, increasing its photocurrent response. The absorption trend is reflected in the external quantum efficiency (EQE) spectra shown in Figure 3b, where differences in the red absorption tails in Figure 3a are also apparent in the EQE. A general trend was observed with the V_{OC} and fill factor (FF) where the increasing V_{OC} or FF is a good predictor of increasing η. With respect to the Y123[20] reference dye, WN3.1 exhibited very comparable efficiencies.

Table 2. Performance Metrics Extracted From J-V Curves of Devices Using D21L6, WN1, WN3, WN3.1, C218, and Y123 Measured Under 100mWcm^{-2} AM1.5G Illumination Intensity[a].

	WN1	WN3	WN3.1	D21L6	C218	Y123
Efficiency (%)	4.9	5.9	6.3	5.3	6.2	6.6
J_{sc} (mA/cm^2)	8.5	10.2	9.7	9.3	10.3	10.1
V_{oc} (mV)	814	830	871	795	834	881
FF	0.71	0.70	0.75	0.71	0.72	0.74

[a]All devices were masked to achieve an illuminated active area of 0.2025 cm^2 with an approximately 2.3μm thick mesoporous TiO_2 layer

To understand the means by which the differences in V_{OC} and FF arise between the dyes, we used transient photovoltage and photocurrent measurements[11] to analyze the electrical properties of the devices. Two likely possibilities were investigated; either a TiO_2 band-edge shift due to dye dipoles or improved electron recombination lifetimes. The effects of band edge shifts due to either dye dipoles[17] or differences in photo-doping of the hole-transporting material (HTM)[20] were compared by measuring capacitance vs. V_{OC}. The capacitance is a measure of the density of trap states (DOS) in the TiO_2 nanoparticle film.[21] Briefly, the capacitance for the transient photovoltage and photocurrent measurements is calculated as

$$C = \frac{\Delta Q}{\Delta V_{OC}},$$

where C is the capacitance, ΔQ is the differential charge generated by an LED pulse, and ΔV_{OC} is the differential change in V_{OC} generated by an LED pulse of the same intensity. In practice, the device is biased with a constant light intensity, ΔQ is calculated by integrating the photocurrent decay of an LED pulse with the device at 0V bias while assuming no recombination losses, and ΔV_{OC} is measured by the photovoltage decay of an LED pulse of the same intensity with the device at 0A current. Given that V_{OC} is a function of light intensity, capacitance at various V_{OC}s can be probed by utilizing a range of baseline light intensities.

Figure 5a shows the V_{OC} vs capacitance dependence of the dyes investigated in this study. Any strictly vertical transformations between the curves could be interpreted as a dye-dipole effect, in which the dipole of a dye shifts the conduction band energy of the TiO_2 and affects the V_{OC}. The limitation of this interpretation was taken to be +/- 20mV to account for errors in the measurement assumptions and fits as well as slight differences in the redox potential of the spiro-OMeTAD due to differences in photo-oxidation. The Y123 reference dye presented a case where the effect of dye dipole on the TiO_2 conduction band was clearly visible. All Y123 data points were vertically separated from those of the other dyes in this study by an amount greater than the +/- 20mV measurement limitation. Due to the fact that the transformations for the other dyes were not strictly vertical and the curves fell within approximately +/- 20mV of each other regardless of slope changes, it was concluded that the observed differences in V_{OC} could not be attributed to differences in dye-dipoles causing TiO_2 conduction band shifts between the other dyes in this study. The WN dyes were noted to have a similar V_{OC} vs. capacitance slope of 136-144mV V_{OC} per decade of capacitance. In contrast, C218 and D21L6 were noted to have a slope of 114-120mV V_{OC} per decade of capacitance (see SI for further information). The different V_{OC} vs. capacitance dependence may be explained as a change in the shape of the TiO_2 DOS.

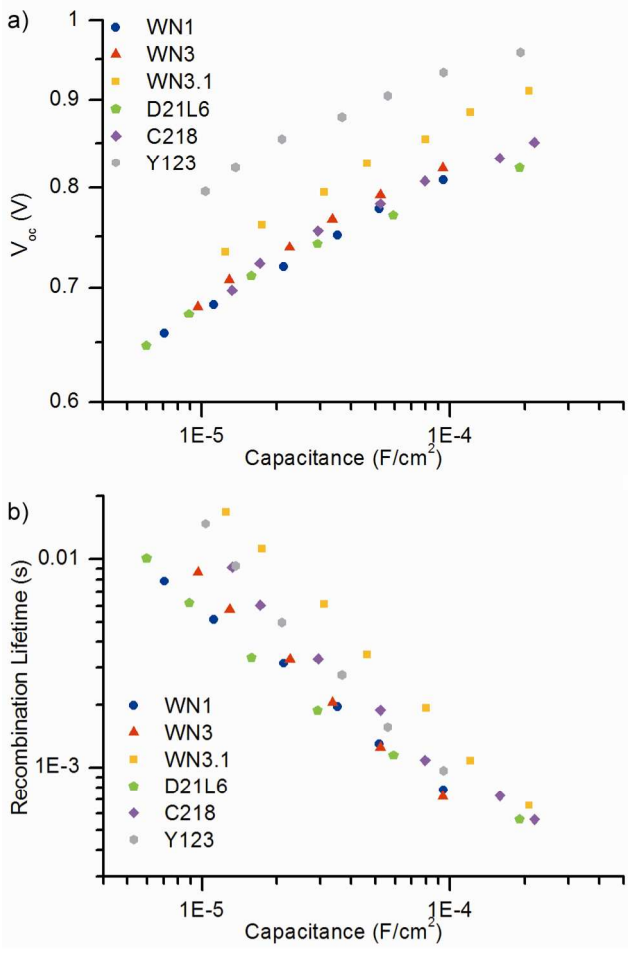

Figure 5. a) Voc vs. capacitance and b) recombination lifetime vs. capacitance of WN1, WN3, WN3.1, D21L6, C218, and Y123 as obtained from transient photovoltage/photocurrent measurements.

Considering that V_{OC} and FF differences could not be explained by TiO_2 conduction band shifts due to dye dipoles, changes to the electron recombination lifetime (τ_{rec}) were also investigated. Briefly, photovoltage decay curves were taken at multiple light intensities (corresponding to multiple capacitances) and τ_{rec} was extracted by monoexponential fits, where τ_{rec} is defined as the characteristic decay constant of the exponential

$$\frac{dV_{OC}}{dt} \propto \exp\left(-t/\tau_{rec}\right),$$

where t is time.

Figure 5b shows the τ_{rec} of the sensitizing dyes measured by transient photovoltage decay as a function of capacitance. At a moderate capacitance near 10^{-5}F, corresponding to an approximate voltage of 700mV (near the max power point) according to Figure 5a, a significant separation in τ_{rec} appeared between the dyes. At this capacitance, WN1/D21L6 had the lowest τ_{rec}, followed by WN3, then C218/Y123, and finally WN3.1. At a high capacitance near 10^{-4}F, corresponding to an approximate voltage of 825mV (near V_{OC}) according to Figure 5a, the recombination lifetimes converged. At this capacitance, WN1/WN3/D21L6 had the lowest and approximately equivalent τ_{rec}, followed by C218/Y123, and then WN3.1. V_{OC}, FF, and η values shown in Table 2 generally follow this trend in τ_{rec}. The apparent relationship between the recombination lifetime of the dyes studied and its effect on efficiency, V_{OC}, and FF of devices can be considered a function of the number of hexyl chains on the dye molecule. WN1 and D21L6, with the lowest τ_{rec}, each have one pair of hexyl chains. WN3 and C218, with an intermediate τ_{rec}, have two pairs of hexyl chains. WN3.1, with the highest τ_{rec}, has three pairs of hexyl chains. A notable exception to this trend is the fact that WN3.1 has a higher τ_{rec} than Y123 even though both dyes have three pairs of hexyl alkyl chains. Whereas WN3.1 places one pair on the donor-group and two on the π-backbone, Y123 has a reversed configuration, with two pairs on the donor and one pair on the π -backbone. We speculate that in addition to the number of alkyl chains, their configuration also plays a role in reducing τ_{rec}.

We hypothesize that the effective steric bulk of the sensitizing dye with respect to the TiO_2 surface is an important parameter affecting the ability of the sensitizing dye to exclude spiro-OMeTAD from the TiO_2 surface and therefore modify the surface recombination rate between these two materials. The quantity of alkyl chains out of the main conjugation plane along the π-backbone of the dye is a good indicator of this steric bulk, which is illustrated for D21L6, Y123, and WN3.1 with a simplistic top-down, donor-to-acceptor view in Figure 6 (Figure SI5 depicts all of the dyes); the green box indicates the conjugation plane of the dye. In this view, D21L6, Y123, and WN3.1 have an increasing amount of alkyl chains extending out of the conjugation plane, respectively, in agreement with the τ_{rec} trend shown in Figure 5b.

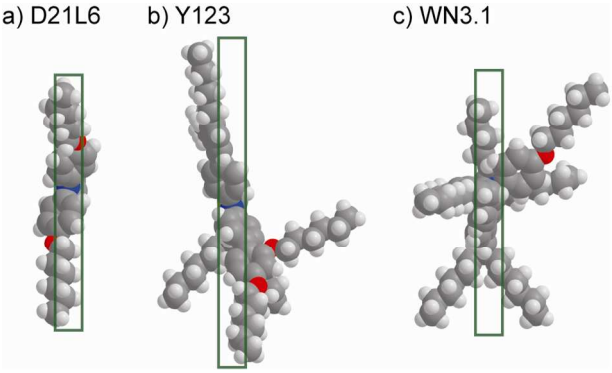

Figure 6. Top-down, donor-to-acceptor, perspective of a) D21L6, b) Y123, and c) WN3.1, as defined by the green arrow in Figure SI6; the green box indicates the conjugation plane along the π-backbone of the dye.

CONCLUSION

This work is important for the further development of DSSC systems where recombination is a problem[8,22–24]. As the recombination lifetime is a significant factor limiting the optimal device thickness and charge collection efficiency in many systems, improving the recombination lifetime via thoughtful placement of additional hexyl chains provides a path towards further efficiency improvements. Although the method employed in this paper resulted in a slight blue-shift of the absorption spectrum of the dyes, it is not expected that the addition of alkyl chains would greatly affect the absorption of the dye in general. In particular, using WN3.1 provides similar device efficiency results to the world record

dye Y123, and we expect slight modifications to WN3.1, i.e. lowering the band gap and increasing dipole, will soon result in world record dyes. Furthermore, this strategy of alkyl group placement may be employed for improving dyes that traditionally perform poorly in ssDSSCs due to fast recombination, such as squaraines[25,26] and phthalocyanines[27], by direct modification of the dye or through co-sensitization with a recombination-blocking D-π-A dye. Further improvements to the recombination lifetime in ssDSSCs by addition and modification of blocking groups on dye molecules will be essential for the development of >10% efficient ssDSSCs utilizing spiro-OMeTAD, and related materials, as the hole-transporting layers.

ASSOCIATED CONTENT

Synthesis and characterization of WN1, WN3, and WN3.1, experimental details of device fabrication and characterization, and raw data of all figures. This material is available free of charge via the Internet at http://pubs.acs.org.

AUTHOR INFORMATION

Corresponding Authors

* mmcgehee@stanford.edu
^ aselli@mines.edu

ACKNOWLEDGMENT

This work was primarily supported by the Office of Naval Research contract # N000141110244. William H. Nguyen was supported by the Department of Defense (DoD) through the National Defense Science & Engineering Graduate Fellowship (NDSEG) Program.

(1) O'Regan, B.; Gra□tzel, M. *Nature* **1991**, *353*, 737–40.
(2) Bach, U.; Lupo, D.; Comte, P.; Moser, J.; Weissörtel, F.; Salbeck, J.; Spreitzer, H.; Grätzel, M. *Nature* **1998**, *395*, 583–585.
(3) Hardin, B. E.; Snaith, H. J.; McGehee, M. D. *Nature Photon.* **2012**, *6*, 162–169.
(4) Hagfeldt, A.; Boschloo, G.; Sun, L.; Kloo, L.; Pettersson, H. *Chem. Rev.* **2010**, *110*, 6595–6663.
(5) Chen, R.; Yang, X.; Tian, H.; Wang, X.; Hagfeldt, A.; Sun, L. *Chem. Mat.* **2007**, *19*, 4007–4015.
(6) Chen, C.-H.; Hsu, Y.-C.; Chou, H.-H.; Thomas, K. R. J.; Lin, J. T.; Hsu, C.-P. *Chemistry* **2010**, *16*, 3184–93.
(7) Bach, U.; Tachibana, Y.; Moser, J. E.; Haque, S. A.; Durrant, J. R.; Grätzel, M.; Klug, D. R. *J. Am. Chem. Soc.* **1999**, *121*, 7445–7446.
(8) Fabregat-Santiago, F.; Bisquert, J.; Cevey, L.; Chen, P.; Wang, M.; Zakeeruddin, S. M.; Grätzel, M. *J. Am. Chem. Soc.* **2009**, *131*, 558–62.
(9) Snaith, H. J.; Schmidt-Mende, L. *Adv. Mater.* **2007**, *19*, 3187–3200.
(10) Ding, I.-K.; Tétreault, N.; Brillet, J.; Hardin, B. E.; Smith, E. H.; Rosenthal, S. J.; Sauvage, F.; Grätzel, M.; McGehee, M. D. *Adv. Funct. Mater.* **2009**, *19*, 2431–2436.
(11) Melas-Kyriazi, J.; Ding, I.-K.; Marchioro, A.; Punzi, A.; Hardin, B. E.; Burkhard, G. F.; Tétreault, N.; Grätzel, M.; Moser, J.-E.; McGehee, M. D. *Adv. Energy Mater.* **2011**, *1*, 407–414.
(12) Li, R.; Liu, J.; Cai, N.; Zhang, M.; Wang, P. *J. Phys. Chem. B* **2010**, *114*, 4461–4.
(13) Kroeze, J. E.; Hirata, N.; Koops, S.; Nazeeruddin, M. K.; Schmidt-Mende, L.; Grätzel, M.; Durrant, J. R. *J. Am. Chem. Soc.* **2006**, *128*, 16376–83.
(14) Paek, S.; Choi, H.; Choi, H.; Lee, C.-W.; Kang, M.; Song, K.; Nazeeruddin, M. K.; Ko, J. *J. Phys. Chem. C* **2010**, *114*, 14646–14653.
(15) Schmidt-Mende, L.; Kroeze, J. E.; Durrant, J. R.; Nazeeruddin, M. K.; Grätzel, M. *Nano Lett.* **2005**, *5*, 1315–20.
(16) Moon, S.-J.; Yum, J.-H.; Humphry-Baker, R.; Karlsson, K. M.; Hagberg, D. P.; Hagfeldt, A.; Sun, L.; Gra□tzel, M.; Nazeeruddin, M. K. *J. Phys. Chem. C* **2009**, *113*, 16816–16820.
(17) Dualeh, A.; Angelis, F. De; Fantacci, S. *J. Phys. Chem. C* **2012**, *116*, 1572–1578.
(18) Frisch, M. J.; Trucks, G. W.; Schlegel, H. B.; Scuseria, G. E.; Robb, M. A.; R.Cheeseman, J.; Scalmani, G.; Barone, V.; Mennucci, B.; Petersson, G. A.; Nakatsuji, H.; Caricato, M.; Li, X.; Hratchian, H. P.; Izmaylov, A. F.; Bloino, J.; Zheng, G.; Sonnenberg, J. L.; Hada, M.; Ehara, M.; Toyota, K.; Fukuda, R.; Hasegawa, J.; Ishida, M.; Nakajima, T.; Honda, Y.; Kitao, O.; Nakai, H.; Vreven, T.; J. A. Montgomery, J.; Peralta, J. E.; Ogliaro, F.; Bearpark, M.; Heyd, J. J.; Brothers, E.; Kudin, K. N.; Staroverov, V. N.; Keith, T.; Kobayashi, R.; Normand, J.; Raghavachari, K.; Rendell, A.; Burant, J. C.; Iyengar, S. S.; Tomasi, J.; Cossi, M.; Rega, N.; Millam, J. M.; Klene, M.; Knox, J. E.; Cross, J. B.; Bakken, V.; Adamo, C.; Jaramillo, J.; Gomperts, R.; Stratmann, R. E.; Yazyev, O.; Austin, A. J.; Cammi, R.; Pomelli, C.; Ochterski, J. W.; Martin, R. L.; Morokuma, K.; Zakrzewski, V. G.; Voth, G. A.; Salvador, P.; Dannenberg, J. J.; Dapprich, S.; Daniels, A. D.; Farkas, O.; Foresman, J. B.; Ortiz, J. V.; Cioslowski, J.; Fox, D. J. *Gaussian Inc., Wallingford CT* **2010**.
(19) Burschka, J.; Kessler, F.; Nazeeruddin, M. K.; Grätzel, M. *Manuscript in preparation*.
(20) Burschka, J.; Dualeh, A.; Kessler, F.; Baranoff, E.; Cevey-Ha, N.-L.; Yi, C.; Nazeeruddin, M. K.; Grätzel, M. *J. Am. Chem. Soc.* **2011**, *133*, 18042–5.
(21) O'Regan, B. C.; Bakker, K.; Kroeze, J.; Smit, H.; Sommeling, P.; Durrant, J. R. *J. Phys. Chem. B* **2006**, *110*, 17155–60.
(22) Yella, a.; Lee, H.-W.; Tsao, H. N.; Yi, C.; Chandiran, a. K.; Nazeeruddin, M. K.; Diau, E. W.-G.; Yeh, C.-Y.; Zakeeruddin, S. M.; Gratzel, M. *Science* **2011**, *334*, 629–634.
(23) Daeneke, T.; Kwon, T.-H.; Holmes, A. B.; Duffy, N. W.; Bach, U.; Spiccia, L. *Nature Chem.* **2011**, *3*, 211–15.

(24) Brennan, T. P.; Bakke, J. R.; Ding, I.-K.; Hardin, B. E.; Nguyen, W. H.; Mondal, R.; Bailie, C. D.; Margulis, G. Y.; Hoke, E. T.; Sellinger, A.; McGehee, M. D.; Bent, S. F. *Phys. Chem. Chem. Phys.* **2012**, *14*, 12130–12140.

(25) Shi, Y.; Hill, R. B. M.; Yum, J.-H.; Dualeh, A.; Barlow, S.; Grätzel, M.; Marder, S. R.; Nazeeruddin, M. K. *Angewandte Chemie* **2011**, *50*, 6619–21.

(26) Geiger, T.; Kuster, S.; Yum, J.-H.; Moon, S.-J.; Nazeeruddin, M. K.; Grätzel, M.; Nüesch, F. *Adv. Funct. Mater.* **2009**, *19*, 2720–2727.

(27) Reddy, P. Y.; Giribabu, L.; Lyness, C.; Snaith, H. J.; Vijaykumar, C.; Chandrasekharam, M.; Lakshmikantam, M.; Yum, J.-H.; Kalyanasundaram, K.; Grätzel, M.; Nazeeruddin, M. K. *Angew. Chem. Int. Ed.* **2007**, *46*, 373–6.